Journal of Integrative Agriculture 2026, 25(9): 3746–3761

Available online at ScienceDirect

Journal of Integrative Agriculture

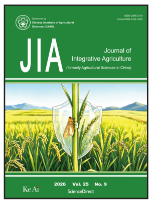

RESEARCH ARTICLE

Development of a performance-matched oxaziclomefone nanosuspension based on the hydrophobic surface characteristics of barnyardgrass for unmanned aerial vehicle sprayers to improve herbicidal activity in direct-seeded rice fields

Xuejian Cheng[1], Chengying Ding[1], Aiping Wang[1], Lidong Cao[1], Chong Cao[1], Pengyue Zhao[1], Manli Yu[1], Li Zheng[2#], Qiliang Huang[1#]

[1] *Institute of Plant Protection, Chinese Academy of Agricultural Sciences, Beijing 100193, China*
[2] *College of Science, China Agricultural University, Beijing 100193, China*

Highlights

- The performance-matched oxaziclomefone nanosuspension (NS), with excellent physical stability suitable for low-volume spraying by unmanned aerial vehicles, was prepared based on the hydrophobic surface characteristics of barnyardgrass.
- The NS significantly decreased the percentage of fine droplets and reduced the potential for droplet drift.
- The NS exhibited superior interfacial performance and remarkably enhanced the uptake and translocation of oxaziclomefone in barnyardgrass.
- Field trials showed that the NS significantly improved the control efficacy of oxaziclomefone against barnyardgrass in direct-seeded rice fields.

Graphical abstract

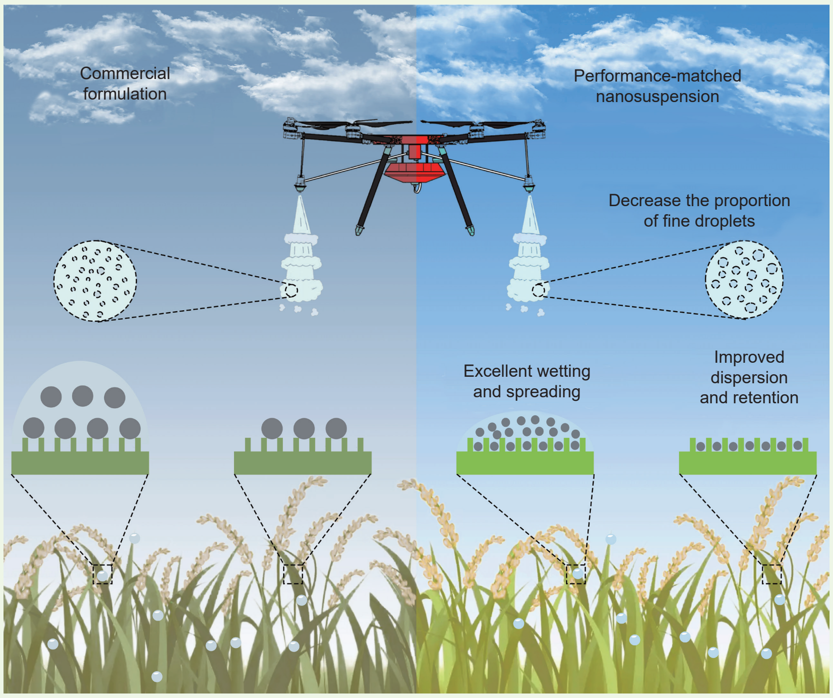

Received 24 March 2025; Received in revised form 21 May 2025; Accepted 8 June 2025; Available online 5 August 2025
[#]Correspondence Li Zheng, E-mail: Zhengli@cau.edu.cn; Qiliang Huang, Tel: +86-10-62816909, E-mail: qlhuang@ippcaas.cn

doi: 10.1016/j.jia.2025.08.003

Abstract

The explosive increase in the use of unmanned aerial vehicle (UAV) sprayers has put forward new requirements for pesticide formulations, and there is an imperative necessity to develop targeted, precise, and efficient pesticide formulations based on the surface characteristics of targets to meet the demand for low-volume spraying by UAVs. Herein, a performance-matched oxaziclomefone nanosuspension (NS) was constructed based on the hydrophobic surface characteristics of barnyardgrass for UAV sprayers. The results showed that the solid surface free energy of the adaxial and abaxial surfaces of barnyardgrass at different growth stages ranged from 23.73 to 28.00 mJ m^{-2} and was dominated by dispersive components. The average sizes of micro-nanostructures on the barnyardgrass surfaces ranged from 251.7 to 266.8 nm, and the oxaziclomefone nanoparticles in the NS could be suitably embedded into the micro-nanostructures of the barnyardgrass surface. The atomization test showed that the NS could significantly decrease the percentage of spray droplets with sizes for droplet drift. Due to the precise regulation of the formulation components, the NS exhibited superior wetting, spreading, and adhesion performance on the barnyardgrass surface. Moreover, the NS remarkably enhanced the uptake and translocation of oxaziclomefone in barnyardgrass. Field trials showed that, compared to the commercial formulation, the NS could significantly improve the control efficacy against barnyardgrass in direct-seeded rice fields while demonstrating acceptable safety for rice. Our research provides a novel, promising, and feasible strategy for the development of pesticide formulations based on target surface characteristics and for improving the physicochemical properties of dilutions, which is valuable for enhancing dosage delivery efficiency and improving control efficiency against pests for UAV sprayers.

Keywords: hydrophobic surface, nanosuspension, unmanned aerial vehicle, herbicidal activity, direct-seeded rice fields

1. Introduction

Population growth and climate change are exacerbating the challenges to global food security (Peng *et al.* 2004; Ray *et al.* 2012; Zhao *et al.* 2017). Rice is one of the most important food crops in the world, fulfilling the carbohydrate demand of over half the world's population (Zhang 2007; Muthayya *et al.* 2014). In recent years, with the reduction of agricultural employment and the rise of cultivation costs, the cultivation pattern of rice has gradually transitioned from labor-intensive transplanting to direct seeding (Panneerselvam *et al.* 2020; Liu *et al.* 2023; Zhang *et al.* 2026). The rice direct seeding pattern has the advantages of saving water, low input demand, and labor savings, which is conducive to the mechanization, intensification, and scaled development of agriculture (Farooq *et al.* 2011; Ohno *et al.* 2018). However, the rice direct seeding pattern is more severely infested with weeds due to the absence of water layers to suppress weed germination and growth (Savary *et al.* 2005; Chauhan *et al.* 2015). Barnyardgrass is one of the most invasive and pernicious weeds in rice fields, causing serious yield losses by competing with rice for water, nitrogen, sunlight, and other resources (Oerke and Dehne 2004; Ottis and Talbert 2017). Currently, herbicides are widely applied *via* post-emergence foliar spray to control barnyardgrass (Deng *et al.* 2021). Unfortunately, the high wax content and micro-nanostructures on the surface of barnyardgrass hinder the deposition, spreading, and penetration of herbicides, resulting in a considerable amount of herbicide wasted into the environment through bouncing, splashing, and rolling off (Sanyal *et al.* 2017; Li *et al.* 2023). The dominant challenge at present is to manage weeds in direct-seeded rice fields economically and efficiently with a smaller environmental footprint and lower herbicide dosage.

Due to advantages such as high operational efficiency, safety for operators, maneuverability, and low labor intensity, unmanned aerial vehicles (UAVs) have been widely used to spray pesticides for pest management in food crop and cash crop fields in East Asia (He *et al.* 2017; Chen *et al.* 2022; Zhou *et al.* 2026). To date, diverse strategies have been proposed for UAV sprayers to enhance dosage delivery efficiency and improve control efficacy against pests. A recent study has shown that decreasing the flight altitude of UAV sprayers can contribute to increased herbicide deposition in the target area when the average wind speed was 1.2–1.5 m s^{-1} (Huang *et al.* 2023). Chen *et al.* (2024) proposed double spraying with two flight sorties routed in length and breadth, which significantly improved the control efficacy of herbicides against grassy and broadleaf weeds in wheat. Additionally, tank-mix adjuvants were added to spray dilutions to enhance pesticide dosage delivery at the leaf surface by decreasing dynamic surface tension, inhibiting droplet rebound, and improving wetting performance (Zhao *et al.* 2022; Wang *et al.* 2024). However, inappropriate tank-mix adjuvant types and concentrations led to a high proportion of fine droplets, which potentially increases the risk of droplet evaporation and drift (Katzman *et al.* 2021; Sun *et al.* 2023). The incompatibility between tank-mix adjuvants and formulations may lead to flocculation, creaming, and precipitation, which is not conducive to uniform spraying and the bioactivity of pesticides (Zhang S *et al.* 2023). Moreover, the complicated operation of preparing spray dilutions and the lack of skilled operators discourage the application of tank-mix adjuvants in agricultural practices. Pesticide formulation optimization for UAV sprayers is a potentially promising and feasible strategy, but to the best of our knowledge, few efforts have been made thus far.

As essential vehicles for pesticide dosage transfer, pesticide formulations can significantly influence the bioactivity of active ingredients (Li *et al.* 2018, 2020). Except for ultra-low volume liquids, most pesticide formulations currently registered and produced globally for spray application are designed for conventional volume spraying. Furthermore, adjuvants in conventional pesticide formulations are screened to safeguard the formation and stabilization of formulations, and little attention is paid to the effect of adjuvants on the physicochemical properties of spray dilutions (Li *et al.* 2015, 2017). The explosive increase in UAV sprayers has put forward new requirements for pesticide formulations, and adjuvants in conventional pesticide formulations must be optimized to be suitable for low-volume spraying with lower dilution ratios. Meanwhile, the higher concentrations of adjuvants in spray dilutions due to the lower dilution ratios of pesticide formulations may result in lower surface tensions and superior deposition, wetting, and spreading performance on the leaf surface. Therefore, the physicochemical properties of spray dilutions can be precisely regulated by pesticide formulation optimization to match the surface characteristics of the target, which has the potential to remarkably improve dosage delivery efficiency and bioactivity against pests.

Nanotechnology-inspired technological breakthroughs and innovations in agriculture are reinvigorating efforts to ensure global food security (Wang *et al.* 2016; Gomez *et al.* 2021; Agrawal *et al.* 2022). Nano-based pesticide formulations are reputed for improved dispersion, enhanced foliar adhesion, excellent stability, targeted delivery, and improved uptake and translocation, which potentially reduce the environmental impact of pesticide application while remarkably improving bioactivity against pests (Nuruzzaman *et al.* 2016; Wang *et al.* 2022; Song *et al.* 2026). Nanosuspension, as a type of non-carrier-coated nano-based pesticide formulation, mainly consists of sub-micron-scale colloidal dispersions of pesticide nanoparticles, surfactants, and dispersants (Corrias *et al.* 2021; Ding *et al.* 2024). Due to the benefits of being organic solvent-free, low-cost, scalable, and having high loading capacity, nanosuspension is promising for extensive practice in agriculture in the foreseeable future (Xiao *et al.* 2019; Iqbal *et al.* 2023). The development of nano-based pesticide formulations suitable for UAV sprayers is in line with the vision of sustainable and smart agriculture, but so far few nano-based pesticide formulations have been designed specifically for UAV sprayers. Moreover, although the improved indoor bioactivity of nano-based pesticide formulations has been widely reported, there is a relative paucity of data evaluating the control efficiency of field applications.

Oxaziclomefone, namely 3-[1-(3,5-dichlorophenyl)-1-methylethyl]-2,3-dihydro-6-methyl-5-phenyl-2H-1,3-oxazin-4-one, is an organic heterocyclic herbicide widely applied to control barnyardgrass in rice fields (O'Looney and Fry 2005). Oxaziclomefone exerts herbicidal activity by inhibiting meristem growth, ultimately causing barnyardgrass necrosis and death (Suzuki *et al.* 2003). Currently, the primary pesticide formulation of oxaziclomefone is suspension concentrate, in which the particle size of oxaziclomefone is on a micron scale, resulting in low dispersion and dosage delivery efficiency. Moreover, suspension concentrates are designed for conventional volume spraying, and the performance of spray dilutions does not match the surface characteristics of barnyardgrass. Therefore, the primary objectives of this research are as follows: (1) characterization of the barnyardgrass leaf surface; (2) development of a performance-matched oxaziclomefone nanosuspension (NS) for UAV sprayers based on the surface characteristics of barnyardgrass; and (3) evaluation of the post-emergence herbicidal activity of NS against barnyardgrass in the field. This research is intended to provide valuable insights into pesticide formulation development for UAV sprayers, which is meaningful for enhancing dosage delivery efficiency and improving control efficiency against pests.

2. Materials and methods

2.1. Materials

Oxaziclomefone technical material (97.0%) was obtained from Liaoning Cynda Chemical Co., Ltd. (Liaoning, China). The 10% oxaziclomefone suspension concentrate (SC) was purchased from Shandong Cynda Chemical Co., Ltd. (Shandong, China). Other chemicals used in the experiment are listed in Appendix A. All chemicals were used as received.

2.2. Characterization of barnyardgrass leaf surface

Cultivation of barnyardgrass Barnyardgrass seeds were germinated for 7 days on cotton gauze soaked with deionized water and then sown into plastic experimental pots (10 cm×10 cm×8 cm) filled with soil (substrates: vermiculite (3:1, v/v)). Subsequently, barnyardgrass was cultivated to the two-leaf and three-leaf stages in an artificial greenhouse at 25°C (80% humidity; light:dark photoperiod (14 h:10 h)).

Scanning electron microscopy of leaf surface Fresh barnyardgrass leaves were adhered to conductive tape. To avoid structural collapse, fresh barnyardgrass leaves were placed at room temperature overnight and dried naturally. After being coated with platinum under vacuum (EM ACE600, Leica, Germany), the micro-nanostructures of the barnyardgrass leaf surface were observed by scanning electron microscopy (SEM, SU8010; Hitachi, Tokyo, Japan) at an acceleration voltage of 10 kV.

Evaluation of the solid surface free energy The solid surface free energy (SFE) of barnyardgrass leaves was evaluated according to the OWRK method (He *et al.* 2021; Lu *et al.* 2021). Fresh barnyardgrass leaves were fixed on slides with double-sided tape, and then the contact angles of water, formamide, ethylene glycol, and DMF on the surface of the barnyardgrass were determined at room temperature using sessile drop mode by an optical contact angle meter (SCA 20; DataPhysics Instruments GmbH) equipped with calculation software SCA 20. The SFE of barnyardgrass leaves was calculated by inputting the contact angle, dispersive component, and polar component of the above four liquids into the SCA20 software. The details of the four test liquids are listed in Appendix B.

2.3. Preparation and optimization of oxaziclomefone nanosuspension

Screening of dispersants Oxaziclomefone nanosuspensions (NS) were prepared by wet media milling (Cheng *et al.* 2024). First, 5 g dispersant and 10.3 g oxaziclomefone technical material powder were dispersed in 79.4 g deionized water under magnetic stirring to form an aqueous dispersion. Second, the above dispersion was transferred to a piece of milling equipment (WG-0.3, Suzhou Vgreen Nano-Chem Technology Co., Ltd., Jiangsu, China) containing 760.2 g of 0.3 mm diameter zirconia beads in the chamber, and milled at 2,000 r min^{-1} for 120 min to obtain nanosuspension. Third, the nanosuspension was mixed with 0.1 g defoamer SAG 1572, 5 g propylene glycol, and 0.2 g xanthan gum for 3 min at 3,000 r min^{-1} using a high-speed shearing machine (Ultra turrax T10 basic, IKA, Germany). Finally, four NSs prepared with PEAS 03, GY1200, GY1150, and Morwet D425 as dispersants were dispensed into well-sealed glass vials, and the optimal dispersant was screened by determining the variation of particle size distribution after accelerated storage stability.

Screening and optimization of wetting agents The equilibrium surface tensions (EST) of wetting agents at the concentrations of 0.001%, 0.005%, 0.01%, 0.05%, 0.1%, 0.5%, 1%, and 2% were measured based on the Wilhelmy plate method using a surface tension instrument (DCAT 21, Data Physics, Germany). Subsequently, NS containing different types of wetting agents were prepared according to the method described above. The mass of the wetting agent was 3 g, and the mass of deionized water was modified to 76.4 g. The optimal wetting agent type was identified by determining the particle size distribution after accelerated storage stability tests. Finally, NS with 1%, 2%, 3%, 4%, and 5% of wetting agents were prepared for the evaluation of physicochemical properties of dilutions, respectively. The characterization details of NS are listed in Appendix C.

2.4. Preparation of spray dilution

The recommended field dosage for oxaziclomefone was 45 g ha^{-1}, and the oxaziclomefone content of NS was 10%, so the NS was applied at 450 g ha^{-1}. The spray volume of the UAV was set to 22.5 L ha^{-1} according to Shan *et al.* (2022). Therefore, the NS was diluted 50-fold with deionized water and stirred vigorously for 1 min to mix the spray dilution for characterization of physicochemical properties. As a control, 10% SC was diluted 50-fold with deionized water.

2.5. Measurement of spray droplet size spectrum

The spray dilutions were atomized by a centrifugal nozzle (Eavision Technologies Co., Ltd., Suzhou, China), and then the spray droplet size spectra were measured by a laser particle sizer (DP-02, OMEC Instruments Co., Ltd., Zhuhai, China) by scanning the complete cross-sectional area of the spray at 0.5 m below the nozzle. The relative span (RS) of droplets was calculated according to eq. (1):

$$RS=\frac{DV_{90}-DV_{10}}{DV_{50}} \quad (1)$$

where DV_{10}, DV_{50}, and DV_{90} are the droplet sizes below which 10%, 50%, and 90% of droplets in the spectrum are smaller, respectively.

The viscosity of NS was measured by a viscometer (NDJ-5S, Shanghai LICHEN-BX Instrument Technology Co., Ltd., China).

2.6. Physicochemical properties of dilution

Surface tension EST of NS dilutions was determined using a surface tension instrument (DCAT 21, Data Physics, Germany) by the Wilhelmy plate method. The dynamic surface tension (DST) of NS dilutions was characterized using a BP100 bubble pressure tensiometer (KRÜSS Ltd., Germany). The range of bubble surface ages was 10 to 5,000 ms, and the capillary diameter was 0.316 mm.

Contact angle and spreading factor The dynamic contact angle of dilutions on the adaxial surface of three-leaf stage barnyardgrass leaves was determined by an optical contact angle meter (SCA 20, Data Physics, Germany) using sessile drop mode at room temperature. Five microliters of dilution were deposited onto the barnyardgrass surface by a syringe pump, and the contact angles and droplet spreading diameters were monitored for 180 s. The contact angle at 180 s was considered the equilibrium contact angle. The spreading factor was defined as the ratio of the droplet spreading diameter at time t to the droplet spreading diameter at 0 s, and the spreading factor at 180 s was considered the equilibrium spreading factor.

Adhesion work The adhesion work (Wa) can be calculated according to eq. (2):

$$Wa=EST\times(1+\cos\theta) \quad (2)$$

where Wa is the adhesion work (J m^{-2}), EST is the equilibrium surface tension (mN m^{-1}) of dilutions, and θ is the equilibrium contact angle (°) of dilutions on the barnyardgrass leaves.

Adhesive force The adhesive force between the dilutions and barnyardgrass leaves was measured by a high-sensitivity balance (DCAT 21, Data Physics, Germany) through the ring method. The three-leaf stage barnyardgrass leaves were fixed to slides using double-sided tape. Ten microliters of dilutions were injected into the ring by a syringe, and the force-distance curves were plotted by recording the interaction force between the dilutions and leaves.

2.7. Deposition morphology

The dilution of NS was deposited on the adaxial surface of barnyardgrass at the three-leaf stage. After being coated with platinum under vacuum (EM ACE600, Leica, Germany), the deposition morphology was observed by scanning electron microscopy (SEM, SU8010; Hitachi, Tokyo, Japan) at an acceleration voltage of 10 kV.

2.8. Uptake and translocation

Twenty microliters of dilutions were dropped onto the adaxial surface of the lower leaves of barnyardgrass at the three-leaf stage. The above-ground part of the barnyardgrass was harvested at 24 and 72 h after treatment. The lower leaves (treated leaves) were collected individually and ultrasonically washed for 2 min with deionized water to assess the uptake of oxaziclomefone by barnyardgrass. The translocation of oxaziclomefone in barnyardgrass was evaluated by determining the concentration of oxaziclomefone in the shoot and upper leaves (untreated part) of barnyardgrass. The concentration of oxaziclomefone in the barnyardgrass was determined by the QuEChERS method combined with high-performance liquid chromatography-tandem mass spectrometry (HPLC-MS/MS). Sample preparation, HPLC-MS/MS conditions, and method validation are listed in Appendix D.

2.9. Field herbicidal activity

Field experiments were conducted in direct-seeded rice fields to investigate the post-emergence herbicidal activity of NS against barnyardgrass in Zhenjiang City, Jiangsu Province, China (Experiment 1) and Changsha City, Hunan Province, China (Experiment 2). The above two experimental sites represent two typical rice-producing areas in China, where Jiangsu is in the rice-wheat rotation mode and Hunan is in the double-cropping rice mode. The spray volume was 22.5 L ha^{-1}, and the applied dosage of oxaziclomefone was 45 g ha^{-1}.

Experiment 1 The field experiment was conducted in July 2024 when the barnyardgrass was at the two-leaf and three-leaf stages. The ambient temperature during the test was 28°C to 30°C, and the wind speed was 1.0 to 2.0 m s^{-1}. The NS was sprayed by a UAV (EA-30XP, Eavision Technologies Co., Ltd., Suzhou, China) with a flight altitude of 2 m, flight speed of 3 m s^{-1}, and an effective working width of 4 m. The droplet size was set as 100 µm. SC was sprayed with the same dosage and operation parameters as a control. Each treatment was conducted in a 1,000 m^2 (16 m×62.5 m) rice field. Each treatment had three plots, and the area of each plot was 333 m^2 (16 m×20.8 m). A 10-m gap between each test field was set as a buffer zone. Meanwhile, a blank treatment (CK) without herbicide application was set. Visual inspection of rice seedling injury was performed 2 weeks after treatment, and the "W" pattern with nine sampling points was used to investigate the control efficiency at 4 weeks after treatment.

The rice seedling injury was assessed according to the following methods: 0%=no injury; 1%–10%=a few seedlings showing abnormal growth symptoms but not noticeable; 11%–20%=rice seedlings on the plot showing noticeable but acceptable abnormal growth symptoms; 21%–30%=rice seedlings on the plot showing noticeable abnormal growth symptoms that would recover with seedling growth; 31%–50%=rice seedlings on the plot showing unacceptable noticeable abnormal growth symptoms that might recover before harvest or not; and >50%=unacceptable rice seedling injury. The weed mortality rate and fresh weight control effect can be calculated according to eqs. (3) and (4).

Weed mortality rate (%)=(The number of weed plants of CK–The number of weed plants of treatment)/The number of weed plants of CK (3)

Fresh weight control effect (%)=(The fresh weight of CK–The fresh weight of treatment)/The fresh weight of CK (4)

Experiment 2 The field experiment was conducted from July to August 2024 when the barnyardgrass was at the two-leaf and three-leaf stages. The ambient temperature during the test was 30°C to 32°C, and the wind speed was 0.3 to 1.5 m s^{-1}. The NS was sprayed by a UAV (T20P, SZ DJI Technology Co., Ltd., Shenzhen, China) with a flight altitude of 1.5 m, flight speed of 3 m s^{-1}, and an effective working width of 4 m. The droplet size was set as 100 µm. SC was sprayed with the same dosage and operation parameters as a control. Each treatment was conducted in a 1,000 m^2 (16 m×62.5 m) rice field. Each treatment had three plots, and the area of each plot was 333 m^2 (16 m×20.8 m). A 10-m gap between each test field was set as a buffer zone. Meanwhile, a blank treatment (CK) without herbicide application was set. Visual inspection of rice seedling injury was performed 1 week after treatment, and rice plant height and fresh weight were investigated 3 weeks after the treatments. After 1 and 3 weeks of treatment, respectively, random sampling was used to investigate the control efficiency in ten sample points. The rice seedling injury, weed mortality rate, and fresh weight control effect were evaluated in the same way as in Experiment 1.

2.10. Statistical analysis

The data were presented as mean±standard deviation of three repetitions. One-way analysis of variance (ANOVA) and independent samples *t*-test were used to analyze the significance of the differences at a significance level of 0.05.

3. Results and discussion

3.1. Characterization of barnyardgrass leaf surface

The deposition, adhesion, wetting, and spreading behaviors of pesticide dilutions on the leaves were influenced by the chemical characteristics and roughness of surfaces (Gao *et al.* 2018; Si *et al.* 2018; Sun *et al.* 2023). Generally, the herbicide is sprayed when the barnyardgrass grows to the two-leaf and three-leaf stages in direct-seeded rice fields for post-emergence control. Thus, the surface characteristics of barnyardgrass at the two-leaf and three-leaf stages were evaluated. The SFE and components of barnyardgrass leaves can be calculated by determining the contact angles of four liquids with different polarities. The surface tension and components of test liquids are listed in Appendix B, and the polarities of the four liquids were ranked in descending order: water>formamide>ethylene glycol>DMF. As illustrated in Fig. 1-A, the contact angles of the four test liquids on the surface of barnyardgrass were significantly different, as evidenced by the fact that the contact angles of polar test liquids (water and formamide) on both the adaxial and abaxial surfaces of barnyardgrass were larger than those of non-polar test liquids (ethylene glycol and DMF). Moreover, the contact angles of the four test liquids on the abaxial surface were smaller than those on the adaxial surface, implying that the abaxial surface was more hydrophilic than the adaxial surface (Table 1). Notably, the contact angles of the four test liquids on the surface of barnyardgrass increased as the barnyardgrass grew, which indicates that the water repellency of barnyardgrass increased as it aged.

According to the data in Fig. 1-B, the SFE of the adaxial and abaxial surfaces decreased as the barnyardgrass aged. Specifically, the SFE of the adaxial surface decreased from 26.78 to 23.73 mJ m^{-2}, and the SFE of the abaxial surface decreased from 28.00 to 24.24 mJ m^{-2}. Zhu *et al.* (2014) also reported that the SFE of rice decreased with plant aging. Previous research has shown that solid surfaces with SFE below 20 mJ m^{-2} were highly hydrophobic, whereas surfaces with SFE in the range of 20 to 40 mJ m^{-2} were

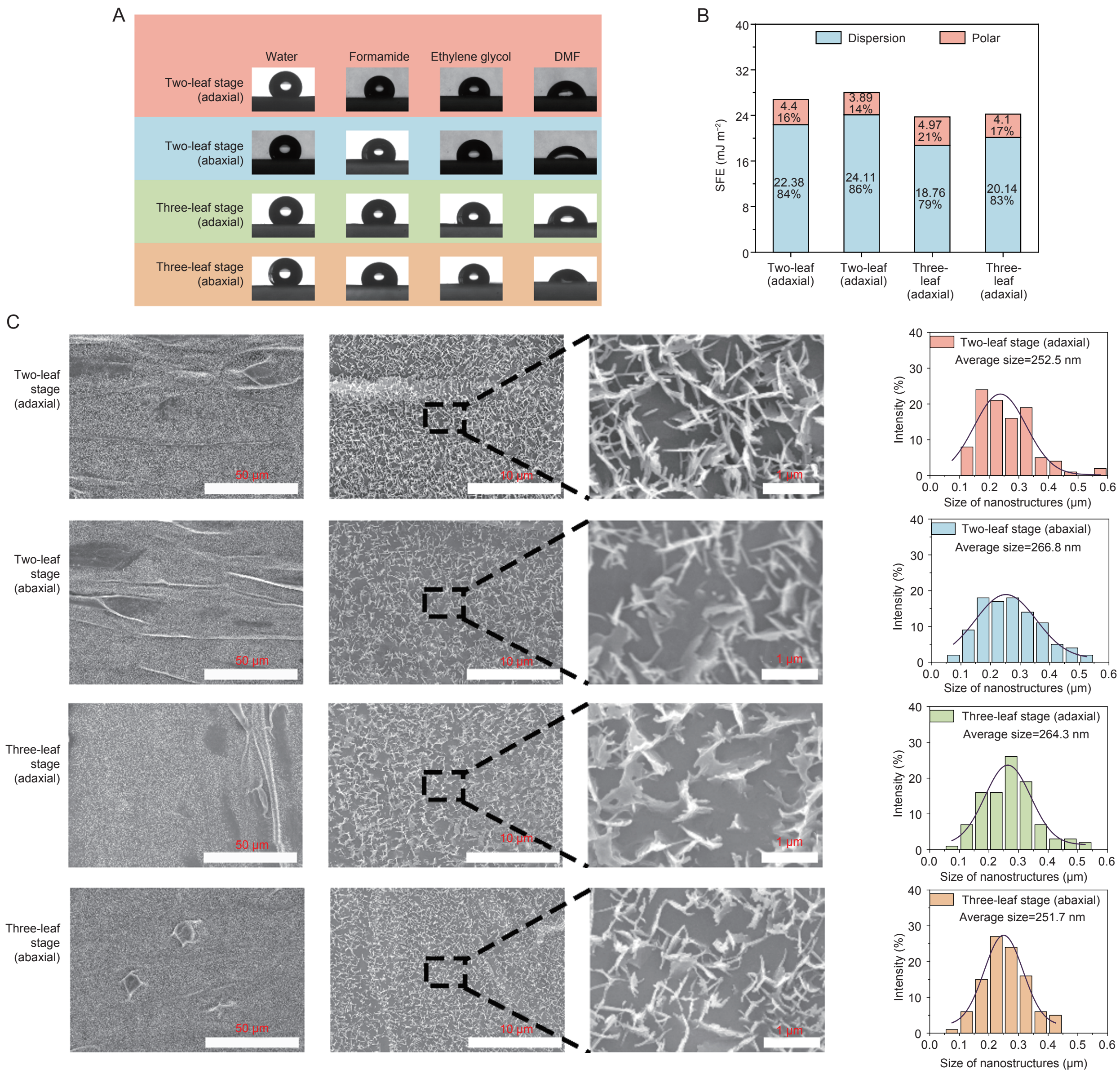

Fig. 1 Characterization of barnyardgrass leaves at the two- and three-leaf stages. A, contact angles of four liquids on the surface of barnyardgrass. B, surface free energy and its components of barnyardgrass. C, scanning electron microscopy (SEM) images of nanostructures on the surface of barnyardgrass and statistical size of nanostructures based on SEM images.

Table 1 Contact angles of the four test liquids on the adaxial and abaxial surface of barnyardgrass in different growth stages

Leaf stage	Leaf part	Contact angles (°)			
		Water	Formamide	Ethylene glycol	N,N-Dimethylformamide
2	Adaxial	129.65±1.90	121.28±4.61	106.87±8.02	73.79±5.33
2	Abaxial	126.69±2.85	114.76±5.64	104.40±4.33	70.63±4.51
3	Adaxial	138.08±1.32	124.57±3.96	113.36±4.64	84.52±1.55
3	Abaxial	133.88±2.87	116.72±5.42	110.69±3.28	81.42±2.56

The data were presented as mean±standard deviation of three repetitions.

hydrophobic (Jiang *et al.* 2023). Therefore, the adaxial and abaxial surfaces of barnyardgrass leaves at the two-leaf and three-leaf stages were hydrophobic. Notably, the SFE of the adaxial surface was lower than that of the abaxial surface, while the proportion of the dispersion component of the adaxial surface was higher than that of the abaxial surface (Fig. 1-B). Considering the similarity of the micro-nanostructures of the adaxial and abaxial surfaces (Fig. 1-C), it can be inferred that the chemical characteristics may be responsible for the above difference. Moreover, the dispersion component decreased as the barnyardgrass grew, and the polar component remained almost constant, which resulted in the polar component accounting for a higher proportion (Fig. 1-B). The percentage of the dispersion component was higher than the polar component at different stages, which indicates that the adaxial and abaxial surfaces were dominated by dispersive components. Recent research has also revealed that the dispersive component was higher than the polar component for tea, wheat, and rice leaves (Zhang *et al.* 2017; Zhu *et al.* 2019; Yang *et al.* 2024).

Fig. 1-C illustrates the morphological characteristics of the barnyardgrass leaf surface at different growth stages. Long ridges were distributed on the rough surface, and papillae could be observed on the abaxial surface of the three-leaf stage barnyardgrass. The high-magnification SEM images showed that the surfaces of barnyardgrass in the two-leaf and three-leaf stages were covered with disordered and dense wax platelets of about 1 μm in length, which divided the surface of barnyardgrass into various micro-nanostructures with different sizes. The sizes of micro-nanostructures were counted based on SEM images using Nano Measurer software, and the results indicated that the average sizes of micro-nanostructures on the two-leaf adaxial, two-leaf abaxial, three-leaf adaxial, and three-leaf abaxial surfaces were 252.5, 266.8, 264.3, and 251.7 nm, respectively. These micro-nanostructures significantly increased the roughness of the barnyardgrass surface and potentially caused air pockets between the droplets and the leaf surface, which hindered the wetting and spreading of droplets (Sun *et al.* 2023). Moreover, the micro-nanostructures on barnyardgrass surfaces were not conducive to the deposition and adhesion of micrometer-scale herbicide. Overall, these results demonstrated that the hydrophobic properties, chemical composition, and micro-nanostructures of barnyardgrass surfaces at different stages were incompatible with the deposition and wetting of pesticide dilutions, which posed a challenge for targeted, efficient, and precise application of herbicides.

3.2. Preparation and optimization of NS

The proper dispersant is crucial for the formation and stabilization of nanosuspensions because the dispersant can be adsorbed onto the surface of the pesticide particles and stabilize the particles by electrostatic repulsion and/or steric hindrance (Wang *et al.* 2013; Ito *et al.* 2016; Tian *et al.* 2022). Therefore, the type of dispersant was screened by the variation in particle size distribution after the accelerated storage stability test. As shown in Fig. 2-A–D, the fresh samples prepared with PEAS 03, GY1200, GY1150, and Morwet D425 as dispersants showed unimodal distribution, which indicates that all the above four dispersants can be applied to prepare NS with uniform particle size distribution by wet media milling. However, the particle size distribution of the NS prepared with PEAS 03, GY1200, and GY1150 as dispersants transformed from unimodal to bimodal after the accelerated storage stability test (Fig. 2-A–C), while the NS prepared with Morwet D425 as the dispersant maintained unimodal distribution after the accelerated storage stability test (Fig. 2-D). The data in Fig. 2-E show that the average particle size of the NS prepared with PEAS 03, GY1200,

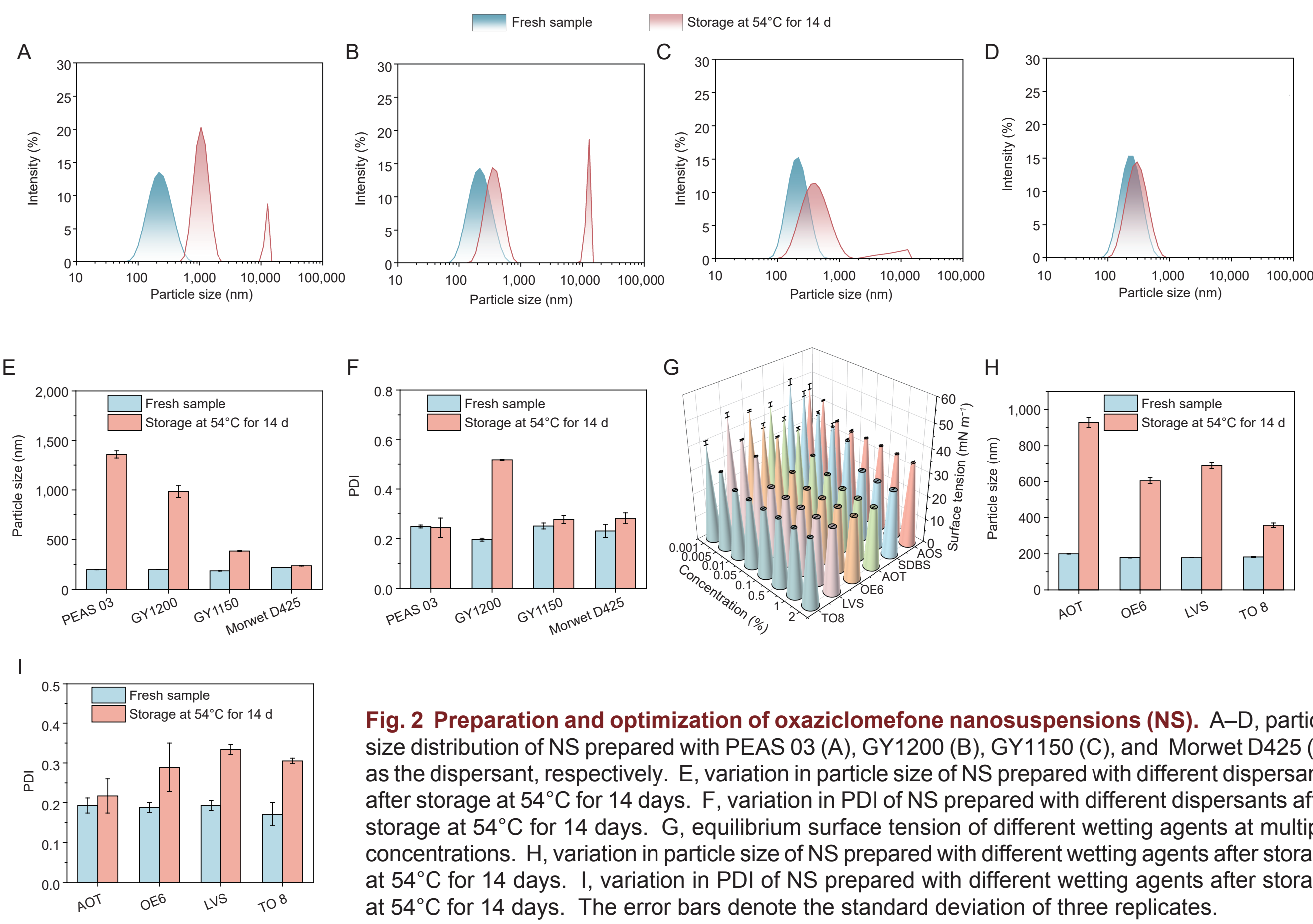

Fig. 2 Preparation and optimization of oxaziclomefone nanosuspensions (NS). A–D, particle size distribution of NS prepared with PEAS 03 (A), GY1200 (B), GY1150 (C), and Morwet D425 (D) as the dispersant, respectively. E, variation in particle size of NS prepared with different dispersants after storage at 54°C for 14 days. F, variation in PDI of NS prepared with different dispersants after storage at 54°C for 14 days. G, equilibrium surface tension of different wetting agents at multiple concentrations. H, variation in particle size of NS prepared with different wetting agents after storage at 54°C for 14 days. I, variation in PDI of NS prepared with different wetting agents after storage at 54°C for 14 days. The error bars denote the standard deviation of three replicates.

GY1150, and Morwet D425 as dispersants increased from the original 197.04, 196.84, 185.06, and 217.15 nm to 1,362.1, 982.1, 385.02, and 236.87 nm after the accelerated storage stability test, respectively. The PDI of NS prepared with PEAS 03, GY1150, and Morwet D425 as dispersants hardly changed (Fig. 2-F). By contrast, the PDI of NS prepared with GY1200 as the dispersant increased from 0.196 to 0.519, which can be attributed to the larger tail in the large size range (Fig. 2-B). Overall, these results indicate that the dispersant Morwet D425 possessed a stronger affinity with oxaziclomefone nanoparticles. Therefore, Morwet D425 was identified as the optimal dispersant for subsequent experiments.

The EST of the dilutions formed by NS diluted with water significantly affects the foliar affinity, and the wetting agent in the formulation is the key factor in regulating this property (Arand *et al.* 2018; Gao *et al.* 2022). Wetting agents act as surfactants that can be absorbed at liquid-vapor and solid-liquid interfaces, lowering the EST of dilutions and thus wetting hydrophobic surfaces (Lee *et al.* 2008; Kovalchuk *et al.* 2016). The critical micelle concentration (CMC) and the EST at CMC (γ_{CMC}) are crucial indexes to evaluate the effectiveness of surfactants in improving the surface activity of dilutions (Gaudin *et al.* 2018). CMC is defined as the concentration at which the surfactant spontaneously forms micelles (Scholz *et al.* 2018). For concentrations lower than CMC, surfactants are distributed both in the bulk and at the interface of dilutions, and with the increase of the concentration, the surfactants both in the bulk and at the interface increase. After the concentrations reach CMC, the surfactant concentration at the interface reaches saturation level, while the excess surfactants in the bulk form micelles (Burlatsky *et al.* 2013). Since EST is governed by the surfactant concentration at the interface, EST no longer decreases appreciably with increasing surfactant concentrations after reaching CMC (Chang *et al.* 2017). A smaller CMC of surfactant means a lower concentration at the interface to reach saturation adsorption, which contributes to the pesticide formulation maintaining a lower surface tension after dilution. The lower the γ_{CMC}, the less work is required for the dilution to form new interfaces, thus potentially wetting more hydrophobic surfaces (Ivanova and Starov 2011). Therefore, considering the hydrophobic nature of barnyardgrass surfaces, it is crucial to screen wetting agents with smaller CMC and lower γ_{CMC} for the preparation of performance-matched NS.

As shown in Fig. 2-G, the approximate CMC of AOS, SDBS, AOT, OE6, LVS, and TO 8 were 0.05%, 0.5%, 0.5%, 0.1%, 0.05%, and 0.05%, respectively. The data in Table 2 show that the γ_{CMC} of AOS, SDBS, AOT, OE6, LVS, and TO 8 were 35.67, 29.15, 25.93, 27.04, 28.69, and 28.05 mN m^{-1}, respectively. Previous research has shown that surfactant solutions with EST higher than 30 mN m^{-1} hardly spread on hydrophobic surfaces (Kovalchuk *et al.* 2016). The γ_{CMC} of AOS was 35.67 mN m^{-1}, so it was hard to wet the hydrophobic barnyardgrass surface even at concentrations up to the CMC. Additionally, the approximate CMC and γ_{CMC} of SDBS were 0.5% and 29.15 mN m^{-1}; thus, the dilutions may be unable to spread on the hydrophobic barnyardgrass surface when SDBS was used as a wetting agent for NS. Therefore, the wetting agents AOT, OE6, LVS, and TO 8 were suitable for further compatibility testing. Fig. 2-H illustrates that the average particle size of AOT, OE6, LVS, and TO 8 increased to 928.68 nm, 604.14 nm, 689.17 nm, and 357.65 nm after the accelerated storage stability test, respectively. The PDI of AOT, OE6, LVS, and TO 8 increased to 0.217, 0.289, 0.334, and 0.305. The results indicate that the wetting agent TO 8 had the best compatibility with the other components in the formulation; thus, TO 8 was identified as the optimal wetting agent for subsequent experiments.

3.3. Characterization of NS

The creaming, flocculation, and precipitation during pesticide formulation dilution increase the risk of nozzle blockage and non-uniform spray (Zhang S *et al.* 2023), so it is necessary to evaluate the dilution stability of NS. As shown in Fig. 3-A, the particle size of NS fluctuated in the range of 190 to 220 nm during 6 h of dilution, and the PDI was less than 0.3. Fig. 3-B shows that the particle size distribution of NS hardly changed after 6 h of dilution. The results indicate that the NS did not undergo obvious Ostwald ripening, coalescence, or flocculation during dilution. Further, the colloidal stability of the dilution was assessed by multiple light scattering. Fig. 3-C illustrates the backscattering profiles of dilutions, where *x*=0 represents the bottom of the dilutions, the *x*-axis scale represents different heights of the dilutions, the *y*-axis scale represents the backscattering light intensity, and the various colors correspond to the backscattering curves at different scanning cycles. The backscattering profiles of the SC dilution show that the backscattering light intensity at the top decreased while that at the bottom increased with time, which can be attributed to the oxaziclomefone particles at the top migrating to the bottom over time. It is evident from Fig. 3-D that after 6 h of dilution, the top of the SC dilution became clarified due to the decrease in the concentration of oxaziclomefone particles. By contrast, the backscattering

Table 2 Details of wetting agents[1)]

Codes	Chemical description	CAS	CMC (%)	γ_{CMC} (mN m^{-1})	Supplier
AOS	Sodium C14-16 olefin sulfonate	68439-57-6	0.05	35.67	Shanghai Macklin Biochemical Co., Ltd.
SDBS	Sodium dodecyl benzene sulfonate	25155-30-0	0.5	29.15	Shanghai Aladdin Biochemical Technology Co., Ltd.
AOT	Dioctyl sulfosuccinate sodium salt	577-11-7	0.5	25.93	Jiangsu Hai'an Petrochemical Company
OE6	Ethoxylated isodecanol	61827-42-7	0.1	27.04	Jiangsu Hai'an Petrochemical Company
Emulan LVS	Fatty alcohol alkoxylates	166736-08-9	0.05	28.69	BASF-YPC Company Ltd.
Lutensol TO 8	C13 oxo alcohol ethoxylates	69011-36-5	0.05	28.05	BASF-YPC Company Ltd.

[1)] CAS, CAS registry number; CMC, critical micelle concentration; γ_{CMC}, equilibrium surface tension at critical micelle concentration.

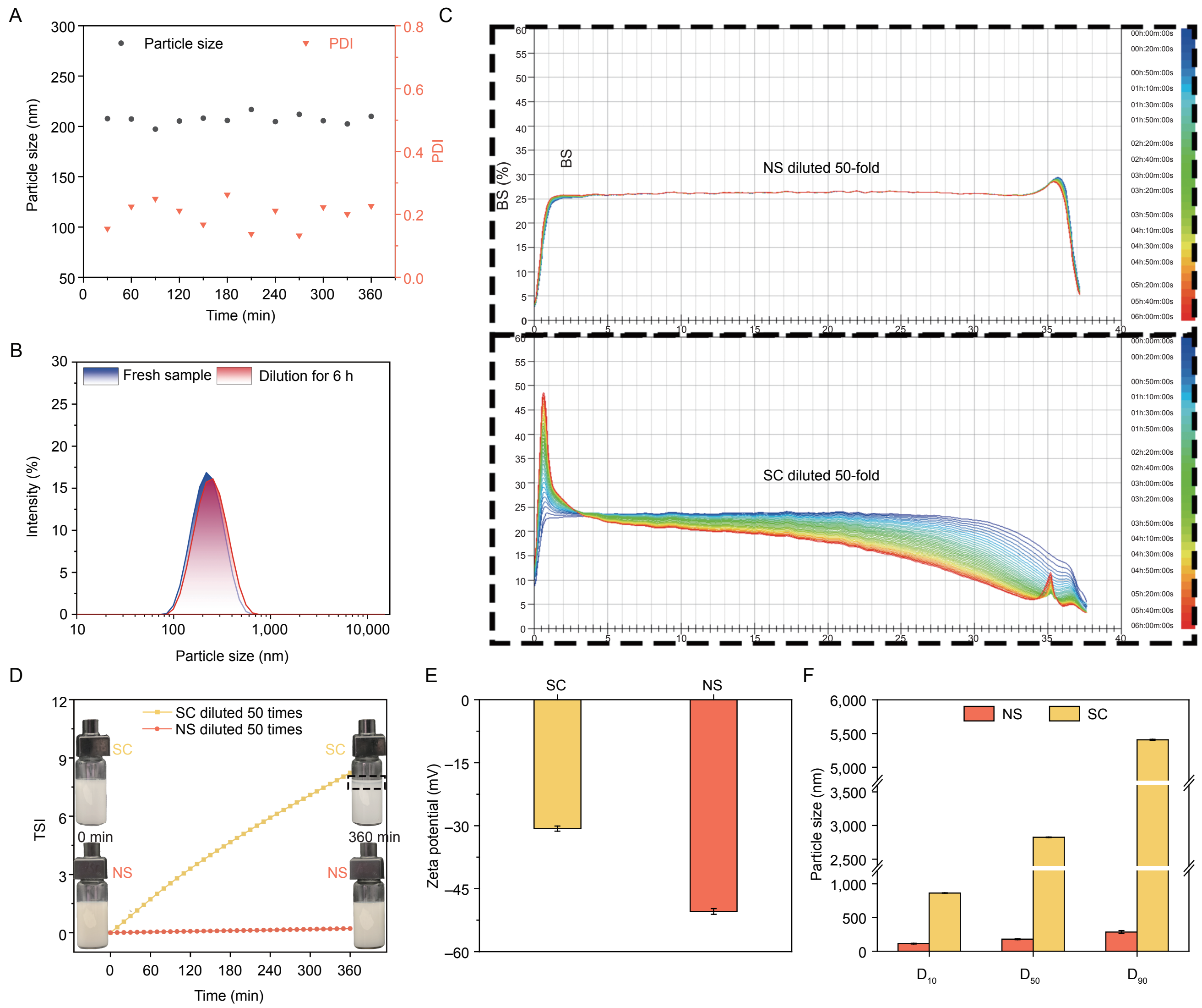

Fig. 3 Characterization of nanosuspension (NS). A, variation of particle size and polydispersity index (PDI) of dilutions over 6 h. B, particle size distribution of NS after dilution for 6 h. C, backscattering profiles of dilutions. D, changes in Turbiscan stability index (TSI) values of dilutions over 6 h. E, zeta potential of NS and suspension concentrate (SC). F, particle size of NS and SC. The error bars denote the standard deviation of three replicates.

light intensity at different heights of the NS dilution hardly changed with time (Fig. 3-C), and there was no significant change in appearance after 6 h of dilution (Fig. 3-D). Moreover, the Turbiscan stability index (TSI) values for the NS dilution were less than 1 during the monitoring period, while the TSI values for the SC dilution increased to 8.23 at 6 h (Fig. 3-D). In general, dispersion systems with smaller TSI values exhibit better colloidal stability (Zheng *et al.* 2018). Therefore, the NS dilution showed superior colloidal stability over the SC dilution. Further, the zeta potentials and particle sizes of NS and SC were compared to reveal the mechanism leading to the above difference. As shown in Fig. 3-E, the zeta potentials of NS and SC were –50.42 and –30.69 mV, respectively. Previous research has shown that suspensions with an absolute zeta potential greater than 30 mV can maintain long-term physical stability (Wang *et al.* 2013), so it can be inferred that zeta potential was not responsible for the difference. As illustrated in Fig. 3-F, the D_{10}, D_{50}, and D_{90} of NS were 113, 179, and 286 nm, while the D_{10}, D_{50}, and D_{90} of SC were 864, 2,826, and 5,406 nm. The sedimentation rate of particles in dispersions is proportional to the square of the particle radius according to Stokes' law (Li *et al.* 2021). The size of oxaziclomefone particles in SC was mostly on the micrometer scale, while the size of oxaziclomefone particles in NS was on the nanoscale, so the sedimentation rate of particles in SC was faster than in NS. Moreover, collisions between water molecules drove the oxaziclomefone nanoparticles in NS to undergo more intense Brownian motion, which countered the sedimentation driven by gravity (Tang *et al.* 2024). Overall, these results indicate that NS exhibited better dilution stability than SC, which potentially contributes to uniform spraying in low-volume spray by UAV.

3.4. Spray droplet size spectrum of NS

As shown in Fig. 4-A and B, the DV_{10} and DV_{50} of NS dilutions were significantly higher than those of the SC dilution.

Moreover, the data in Fig. 4-C and D illustrate that the DV_{90} and RS of NS dilutions and SC dilution were not statistically significantly different. RS is generally used as an index to evaluate the uniformity of the droplet size, with a smaller RS representing more uniform atomization (Zhang and Xiong 2021). These results indicate that compared to SC, NS can significantly decrease the percentage of fine droplets without increasing the risk of uneven atomization. Further, Fig. 4-E illustrates that NS dilutions significantly decreased the percentage of spray droplet size). Spray droplets with a size , and exhibit more sensitivity to ambient wind speed, temperature, and humidity. Therefore, spray droplets with a size *et al.* 2023). The $DV_{<100μm}$ of SC dilutions was 35.98%, while the $DV_{<100μm}$ of NS dilutions ranged from 24.77 to 25.58%. Thus, these results indicate that NS can significantly decrease the drift potential of droplets. To further reveal the reasons for the above differences, the viscosities of NS and SC were determined. The results showed that the viscosity of SC was 236 mPa s, while the viscosities of NS were all higher than 1,000 mPa s (Fig. 4-F). Obviously, it is the xanthan gum in the NS that increased the viscosity of dilutions, thereby increasing DV_{50} and decreasing the $DV_{<100μm}$. Previous research has shown that the DV_{50} increased with the increase of xanthan gum concentration in the dilutions (Wang *et al.* 2018). Notably, there was no significant difference in DV_{10}, DV_{50}, DV_{90}, RS, $DV_{<100μm}$, and viscosity of NS dilutions with different concentrations of wetting agent TO 8, which implies that the concentration of wetting agent TO 8 did not have a significant effect on spray size spectrum.

3.5. Physicochemical properties of dilution

The physicochemical properties of pesticide dilutions significantly influence the interfacial behaviors of droplets on the target surface (Li *et al.* 2020; Sun *et al.* 2023). Therefore, the NS with 1%, 2%, 3%, 4%, and 5% of wetting agent TO 8 were prepared for the evaluation of physicochemical properties of dilutions. After NS were diluted 50-fold with deionized water according to the dilution ratio of UAV low-volume spray, the concentrations of TO 8 in the dilutions were 0.02%, 0.04%, 0.06%, 0.08%, and 0.1%, respectively. As shown in Fig. 5-A, the EST of SC was 38.89 mN m^{-1}, which was significantly higher than those of NS. Moreover, as the concentration of TO 8 increased, the EST of NS first decreased significantly and then remained stable. The difference in EST of NS containing 3%, 4%, and 5% TO 8 was insignificant, which can be attributed to the concentration of TO 8 in the dilutions formed by the above three NS being higher than the CMC of TO 8. Previous research has shown that the EST decreases with the increase of surfactant concentration, and then remains constant when the concentration reaches CMC (Cárdenas *et al.* 2024). The data in Fig. 5-B illustrate that the DST of NS exhibited a swifter decrease than SC. Notably, the decrease rate of DST was more rapid with increasing concentrations of TO 8, which can be attributed to more surfactant molecules of TO 8 migrating from the bulk to the air-liquid interface. As shown in Fig. 5-C and D, the contact angle of SC decreased from 125.57° at 0 s to 116.5° at 180 s, which indicates that SC had a weak wetting ability on the adaxial surface of three-leaf stage barnyardgrass leaves even at a low dilution ratio. In addition, the contact angle only exhibited slight decreases in 180 s when the concentrations of TO 8 were 1% and 2% in NS. In contrast, when the concentrations of TO 8 were 3%, 4%, and 5% in NS, the contact angle decreased rapidly to near the equilibrium value within approximately 60 s, and reached 70.8°, 69.36°, and 70.08° at 180 s, respectively. The data in Fig. 5-E illustrate that the spreading factor of SC hardly changed within 180 s, which implies that it was difficult for SC to overcome the pinning effect and spread on the surface of barnyardgrass leaves. Similar to the contact angle results, the spreading factors increased slightly in 180 s when the concentrations of TO 8 were 1% and 2% in NS. However, as the concentration of TO 8 in NS increased to 3%, 4%, and 5%, the spreading factors increased rapidly and reached 1.25, 1.23, and 1.29 at 180 s, respectively. The equilibrium contact angle of NS on the adaxial surface of three-leaf stage barnyardgrass leaves first decreased and then remained constant with increasing TO 8 concentration (Fig. 5-F). Moreover, Fig. 5-G illustrates that the equilibrium spreading factors of NS and SC were not significantly different when the

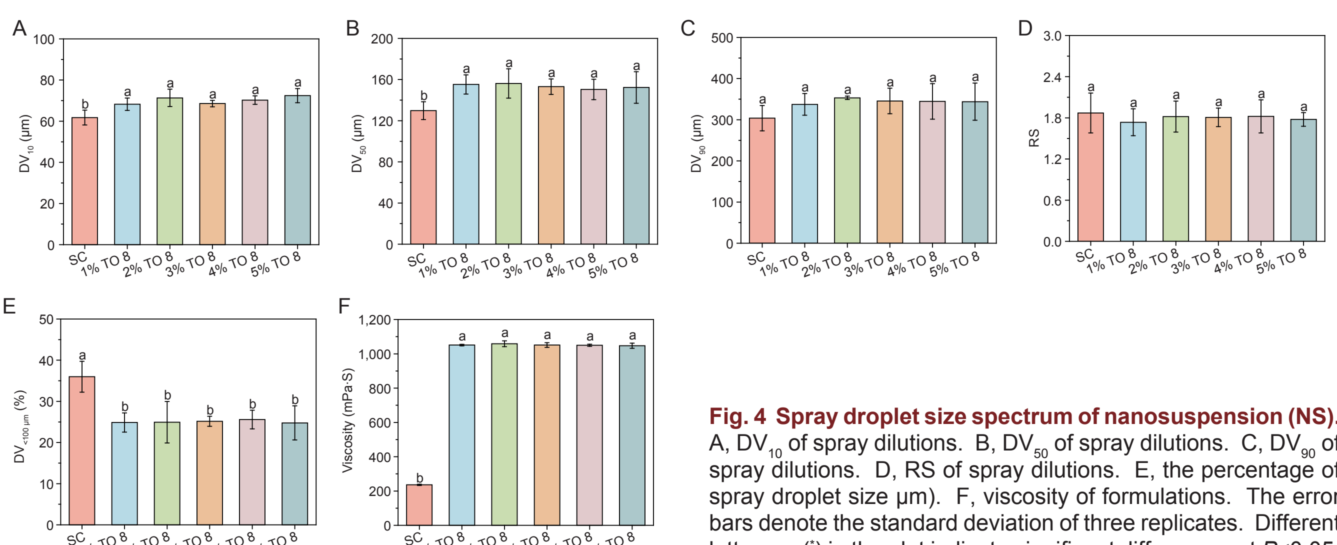

Fig. 4 Spray droplet size spectrum of nanosuspension (NS). A, DV_{10} of spray dilutions. B, DV_{50} of spray dilutions. C, DV_{90} of spray dilutions. D, RS of spray dilutions. E, the percentage of spray droplet size μm). F, viscosity of formulations. The error bars denote the standard deviation of three replicates. Different letters or (*) in the plot indicate significant differences at $P<0.05$.

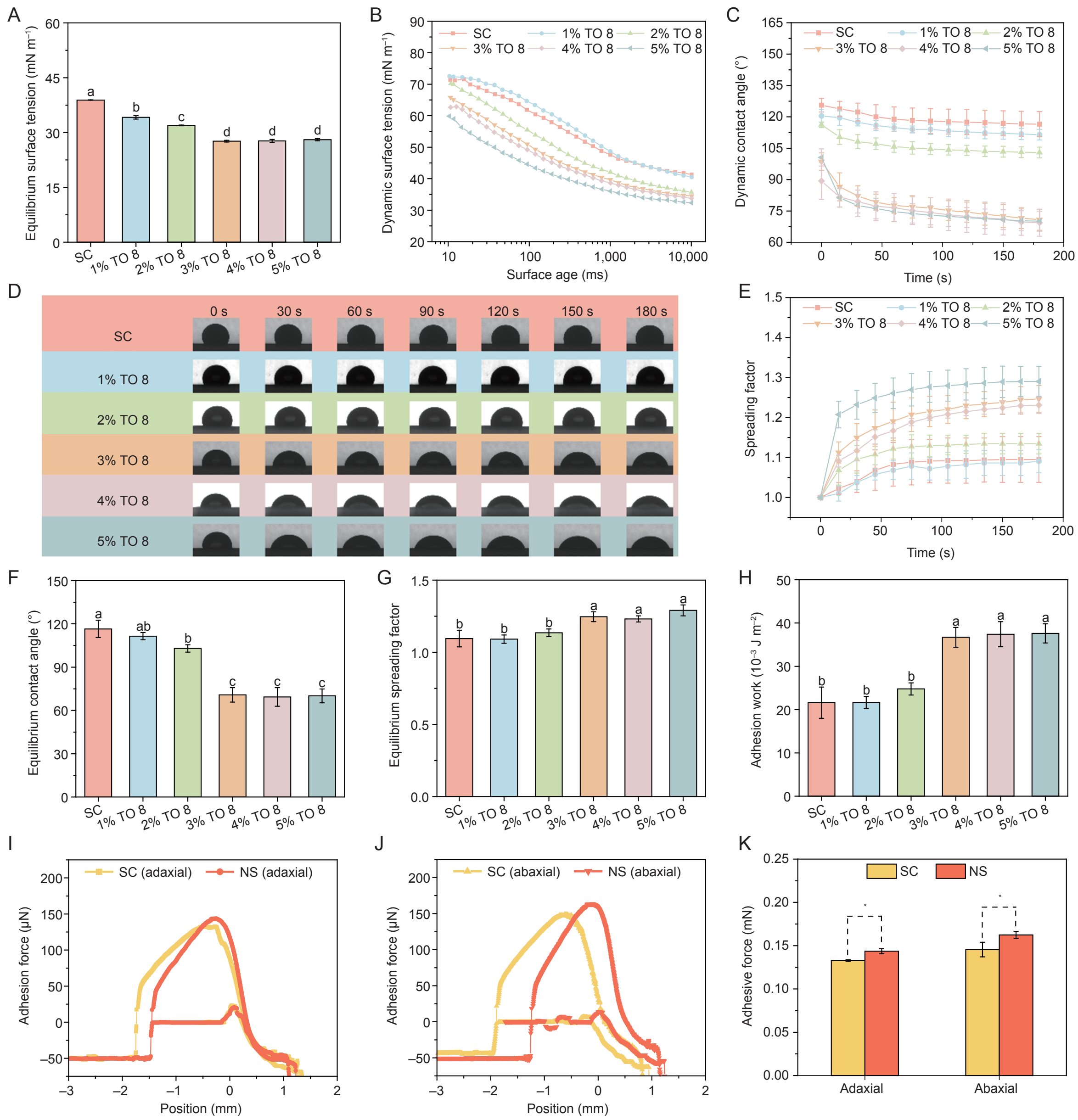

Fig. 5 Wetting and adhesion performances of nanosuspension (NS) dilutions on the surface of barnyardgrass at the three-leaf stage. A, equilibrium surface tension. B, dynamic surface tension. C, dynamic contact angle. D, dynamic contact angle images. E, spreading factor. F, equilibrium contact angle. G, equilibrium spreading factor. H, adhesion work. I, force-distance curves of dilutions on the adaxial surface of barnyardgrass. J, force-distance curves of dilutions on the abaxial surface of barnyardgrass. K, maximum adhesive force of NS dilutions on the barnyardgrass surface. The error bars denote the standard deviation of three replicates. Different letters or (*) in the plot indicate significant differences at P<0.05.

concentrations of TO 8 were 1% and 2%, while the equilibrium spreading factors of NS were significantly higher than those of SC when the concentrations of TO 8 were 3%, 4%, and 5%. In addition, the adhesion work of NS was significantly higher than that of SC when the concentration of TO 8 was 3% in NS (Fig. 5-H). The adhesion work reflects the strength of interaction between the droplets and the leaf surface, and higher adhesion work means stronger adhesion of the droplets to the leaf surface (Zhao *et al.* 2022). These results indicate that NS can exhibit superior wetting, spreading, and adhesion behaviors on the adaxial surface of three-leaf stage barnyardgrass leaves when the concentration of TO 8 was 3%, and thus the optimal concentration of TO 8 in NS was set as 3%. The superior physicochemical properties of NS improved the contact area between the droplets and the barnyardgrass leaves, which potentially promotes the uptake of oxaziclomefone by barnyardgrass.

Furthermore, the maximum adhesive forces between the droplets and three-leaf stage barnyardgrass leaves were measured. As illustrated in Fig. 5-I and J, the maximum adhesion forces of NS on the adaxial and abaxial surfaces of barnyardgrass were larger than those of SC, and the difference was statistically significant (Fig. 5-K). In general, the larger the maximum adhesion force, the stronger the droplets bond to the leaf surface (Bao *et al.* 2022). Therefore, the results imply that the NS showed better adhesion performance on barnyardgrass surfaces than SC.

3.6. Mechanism of performance matching between particle size of NS and barnyardgrass surface micro-nanostructures

The sizes of NS, SC, and micro-nanostructures of barnyardgrass surface were counted based on SEM images using Nano Measurer software to further reveal the mechanism of performance matching between particle size of NS and barnyardgrass surface micro-nanostructures. The oxaziclomefone nanoparticles in NS were monodisperse with irregular polyhedral shapes, and no obvious aggregation was observed among the nanoparticles (Fig. 6-A). Fig. 6-B illustrates that the oxaziclomefone particles in SC exhibited a similar dispersed morphology to NS, but the particle sizes were mostly on the micrometer scale. As shown in Fig. 6-C, the surface of barnyardgrass was covered with micro-nanostructures of different sizes. Further statistics reveal that the sizes of NS, SC, and micro-nanostructures of barnyardgrass surface were 188.6, 2,419.7, and 258.8 nm (Fig. 6-D–F). The deposition morphology of NS in Fig. 6-G illustrates that the oxaziclomefone nanoparticles were suitably embedded into the micro-nanostructures of barnyardgrass surface. By contrast, the oxaziclomefone particles in SC were too large to be embedded into the micro-nanostructures of barnyardgrass surface, and the insufficient contact was not conducive to the retention of herbicides (Fig. 6-H). The size distribution and number fitting curve in Fig. 6-I indicate that the size of the nanoparticles in NS was smaller than the size of the micro-nanostructures of barnyardgrass surface, so most of the nanoparticles in NS can be embedded in the micro-nanostructures of barnyardgrass surface. Zhao *et al.* (2019) designed hat-shaped Janus carriers based on micropapillae and nanosplinters on the rice and wheat leaf surface, which can significantly enhance the retention and flush resistance of pesticides (Zhao *et al.* 2019). Recent research also reported that the retention and adhesion of pyraclostrobin on tomato leaf surfaces can be significantly improved by designing nanocapsules with a flexible topology (Yu *et al.* 2024). These studies revealed the performance matching mechanism between the pesticide and the target surface from the perspective of carrier design strategy. The results of our study revealed the performance matching mechanism between the pesticide and the target surface from the perspective of the size of pesticide dispersion and micro- and nanostructure size of the target surface, which provided a novel, promising, and achievable strategy for designing target affinity pesticide formulations.

3.7. Uptake and translocation of NS

Oxaziclomefone is a systemic herbicide, which can be absorbed by roots and leaves and systemically distributed in the barnyardgrass by translocation (Suzuki *et al.* 2003). To further evaluate the uptake and translocation of NS, the concentrations of oxaziclomefone in barnyardgrass were determined after 24 and 72 h treatment. As shown in Fig. 7-A, the concentrations of oxaziclomefone in treated leaves of NS were not significantly different from those of the SC after 24 and 72 h. However, the data in Fig. 7-B illustrate that the concentration of oxaziclomefone in the untreated part of NS was 66.31 mg kg^{-1} after 24 h treatment, while the concentration of oxaziclomefone in the untreated part was 37.19 mg kg^{-1} after 24 h treatment with SC. Similarly, after 72 h of treatment, the concentration of oxaziclomefone in the untreated part of NS was significantly higher than that of SC (Fig. 7-B). These results indicate that NS exhibited superior uptake and translocation performance in barnyardgrass, and remarkably enhanced the translocation of oxaziclomefone from the treated leaves to the untreated part, which potentially contributes to the systemic distribution of oxaziclomefone in barnyardgrass and improves herbicidal activity.

3.8. Field herbicidal activity of NS

After comprehensively characterizing the physicochemical properties of the dilutions, field experiments were carried out by UAV sprayer to further evaluate the field herbicidal activity against barnyardgrass and safety for rice of NS. Fig. 8-A illustrates the spraying route of UAV sprayers. After 4 weeks of treatment in Jiangsu, the weed mortality rates of NS and SC were 94.44% and 77.78%, respectively (Fig. 8-B). Moreover, the fresh weight control effect shows that the NS treatment was significantly more effective than the SC treatment (Fig. 8-B). In addition, visual inspection results showed that there was no obvious rice seedling injury after being treated with SC and NS, which indicates that NS can improve the control efficacy against barnyardgrass while safeguarding the safety of rice seedlings in Jiangsu.

As shown in Fig. 8-C, the fresh weight control effect of NS was significantly higher than SC after 1 week of treatment in Hunan. The weed mortality rates of NS and SC were 60.57% and 51.12%, but there was no statistically significant difference. Notably, visual inspection showed that rice seedlings on the plot exhibited noticeable but acceptable abnormal growth symptoms after 1 week of NS and SC treatments. As shown in Fig. 8-D–F, the rice seedlings exhibited dwarfing symptoms, and the newly grown leaves displayed yellowing symptoms after 1 week of NS and SC treatments. However, the NS-treated rice seedlings did not show more severe injuries than the SC treatment. The data in Fig. 8-G showed that after 3 weeks of treatment in Hunan, the weed mortality rates of NS and SC were 89.46% and 72.89%, and the fresh weight control effects of NS and SC were 91.87% and 86.17%, which indicates that NS can significantly improve the field herbicidal activity against barnyardgrass compared to SC. Nevertheless, Fig. 8-H and I illustrate that after 3 weeks of SC and NS treatments, the rice plant height and fresh weight were significantly lower than CK. There was no significant difference in rice plant height and fresh weight between SC and NS treatments, which implies that NS did not increase the risk of rice seedling injury compared to SC.

Overall, these results indicate that NS can significantly improve the control efficacy against barnyardgrass while demonstrating acceptable safety for rice. The remarkable improvement can be ascribed to the superior wetting, spreading, and adhesion of the NS dilution, as well as the

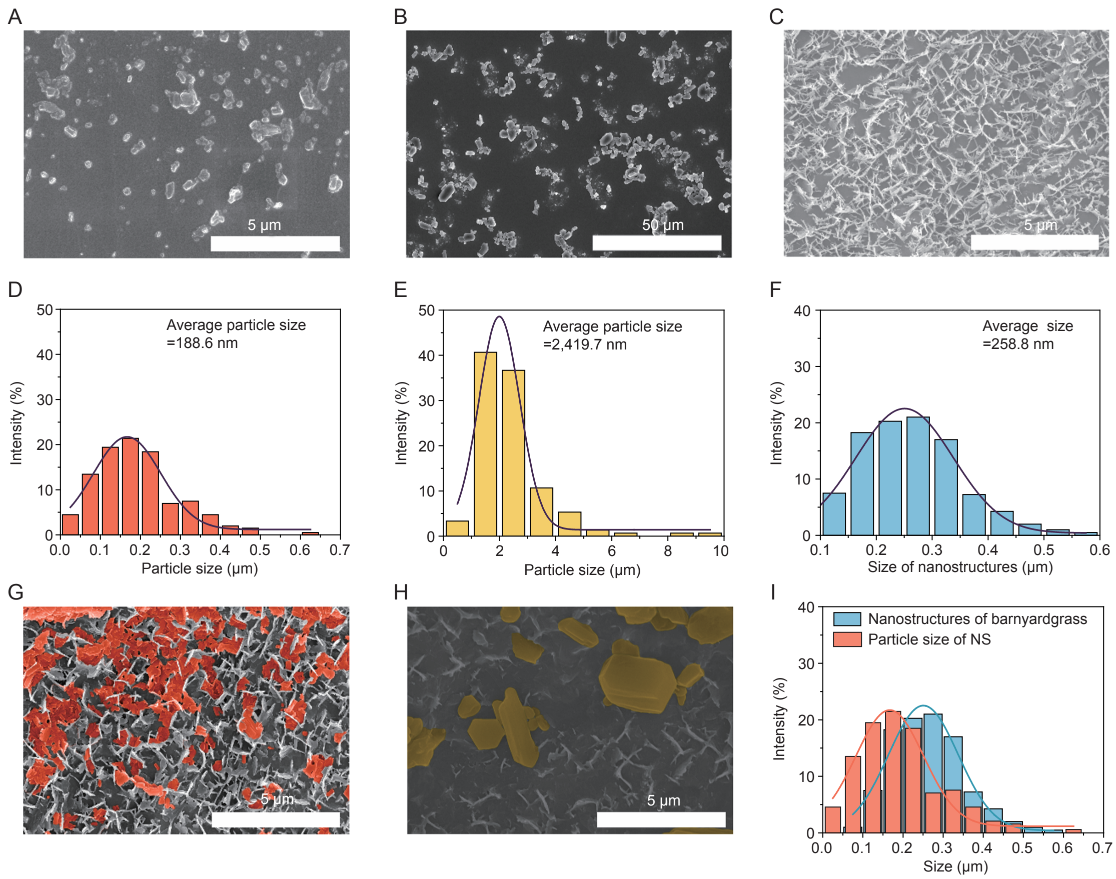

Fig. 6 Mechanism of performance matching between nanosuspension (NS) particle size and barnyardgrass surface micro-nanostructures. A, SEM images of NS. B, SEM images of suspension concentrate (SC). C, SEM images of barnyardgrass surface micro-nanostructures. D, statistical particle size of NS based on SEM images. E, statistical particle size of SC based on SEM images. F, statistical size of barnyardgrass surface nanostructure based on SEM images. G, deposition morphology of NS on the barnyardgrass surface. H, deposition morphology of SC on the barnyardgrass surface. I, matching of NS particle size and barnyardgrass surface nanostructure.

enhanced uptake and translocation of oxaziclomefone nanoparticles in barnyardgrass. Previous studies have shown that nanosuspensions can improve the retention and accumulation of insecticide (imidacloprid) and fungicide (zoxamide) in plant leaves, thereby improving the biological activity against targets (Corrias *et al.* 2021; Iqbal *et al.* 2023). Our findings are consistent with the above studies and further confirm the potency of nanosuspensions in improving herbicide delivery efficiency. Crucially, nanosuspensions feature significant advantages over other nanoformulations such as nanocapsules and nanoliposomes in terms of cost and process stability, and potentially enable large-scale production in the near future. On the one hand, nanosuspensions are sub-micron-scale colloidal dispersions of pesticide nanoparticles (NPs) stabilized by surfactants, polymers, or a mixture of both (Shegokar and Muller 2010), which means that nanosuspensions are low-cost as no additional polymer materials or nanomaterials are required within the formulation. On the other hand, nanosuspensions can be formulated with high production efficiency, scalability, and reproducibility using methods such as wet media milling, high-pressure homogenization, and microfluidization (Van Eerdenbrugh *et al.* 2008; Tian *et al.* 2022), which provides feasibility for wide-scale application of nanosuspensions in sustainable agriculture.

4. Conclusion

In summary, this study developed performance-matched NS based on the hydrophobic surface characteristics of barnyardgrass for UAV sprayers. The OWRK method indicates that the adaxial and abaxial surfaces of barnyardgrass at different growth stages were hydrophobic and dominated by dispersive components. The average

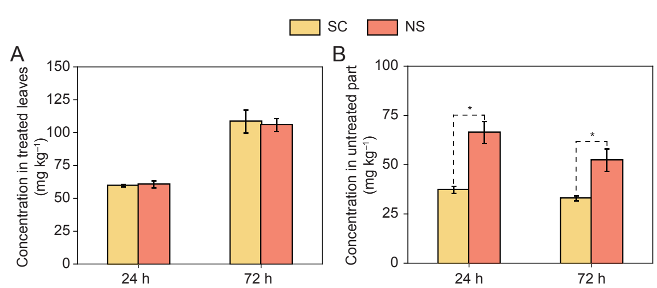

Fig. 7 Uptake and translocation of nanosuspension (NS) in barnyardgrass. A, concentration of oxaziclomefone in treated leaves. B, concentration of oxaziclomefone in untreated parts. SC, suspension concentrate. The error bars denote the standard deviation of three replicates. Different letters or (*) in the plot indicate significant differences at $P<0.05$.

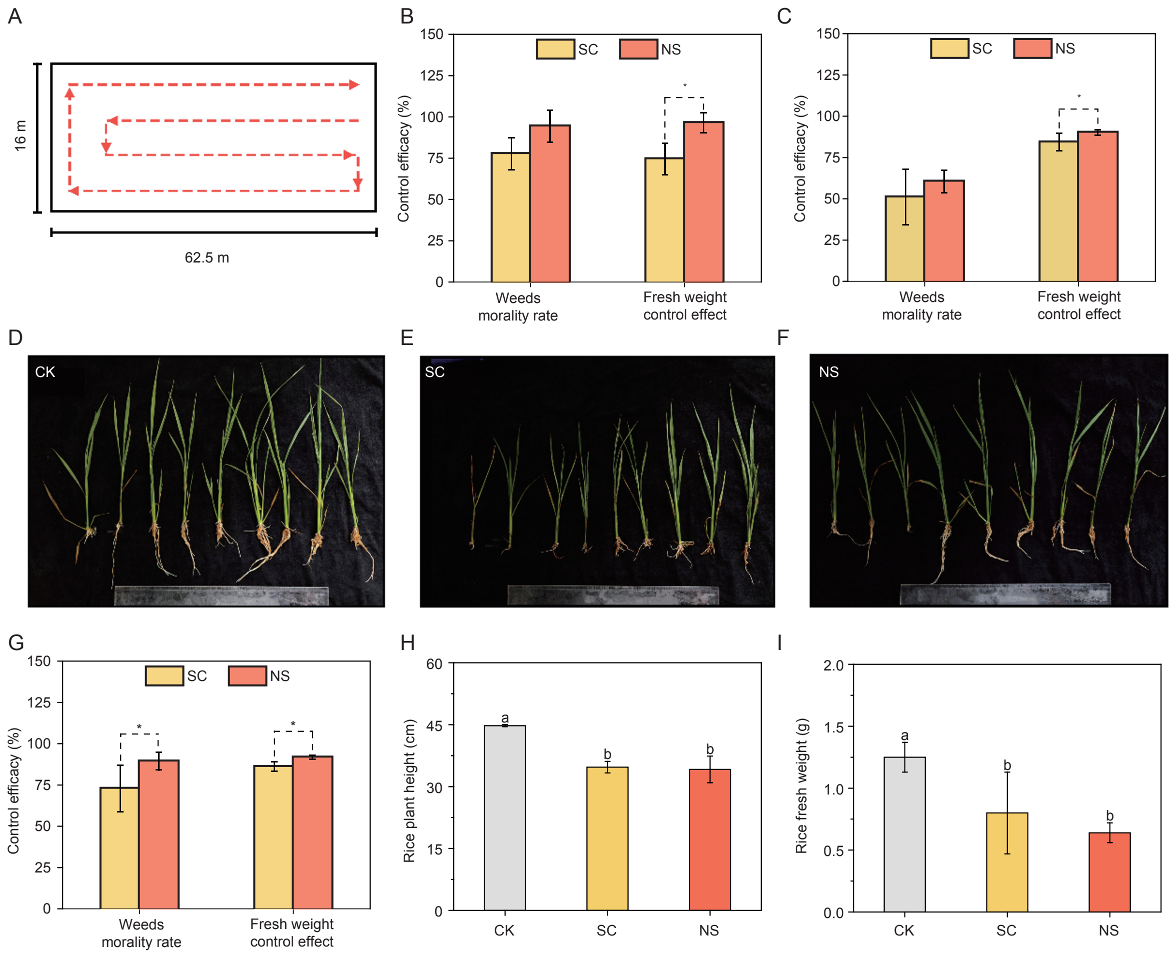

Fig. 8 Field herbicidal activity and safety for rice. A, spraying route. B, control efficacy against barnyardgrass after 4 weeks of treatment in Jiangsu. C, control efficacy against barnyardgrass after 1 week of treatment in Hunan. D, morphological appearances of untreated rice. E, morphological appearances of rice after being treated with suspension concentrate (SC) for 1 week. F, morphological appearances of rice after being treated with nanosuspension (NS) for 1 week. G, control efficacy against barnyardgrass after 3 weeks of treatment in Hunan. H, rice plant height after 3 weeks of treatment in Hunan. I, rice fresh weight after 3 weeks of treatment in Hunan. The error bars denote the standard deviation of three replicates. Different letters or (*) in the plot indicate significant differences at $P<0.05$.

particle size of oxaziclomefone nanoparticles in NS was 188.6 nm, which can suitably be embedded into the micro-nanostructures of the barnyardgrass surface. The NS exhibited excellent dilution stability and storage stability, and superior wetting, spreading, and adhesion performance on the barnyardgrass surface, as well as enhanced uptake and translocation of oxaziclomefone in barnyardgrass. More importantly, the NS can significantly decrease the percentage of spray droplets formulations based on target surface characteristics and for improving the physicochemical properties of dilutions, which is of great significance for enhancing the dosage delivery efficiency and improving the control efficiency against pests for UAV sprayers.

Acknowledgements

This study was supported by the National Key Research and Development Program of China (2022YFD1700500).

Declaration of competing interest

The authors declare that they have no conflict of interest.

Declaration of generative AI and AI-assisted technologies in the writing process

During the preparation of this manuscript, generative AI and AI-assisted technologies were not used.

Appendices associated with this paper are available at https://doi.org/10.1016/j.jia.2025.08.003

References

Agrawal S, Kumar V, Kumar S, Shahi S K. 2022. Plant development and crop protection using phytonanotechnology: A new window for sustainable agriculture. *Chemosphere*, **299**, 134465.

Arand K, Asmus E, Popp C, Schneider D, Riederer M. 2018. The mode of action of adjuvants-relevance of physicochemical properties for effects on the foliar application, cuticular permeability, and greenhouse performance of pinoxaden. *Journal of Agricultural and Food Chemistry*, **66**, 5770–5777.

Bao Z, Wu Y, Song R, Gao Y, Zhang S, Zhao K, Wu T, Zhang C, Du F. 2022. The simple strategy to improve pesticide bioavailability and minimize environmental risk by effective and ecofriendly surfactants. *Science of the Total Environment*, **851**, 158169.

Burlatsky S F, Atrazhev V V, Dmitriev D V, Sultanov V I, Timokhina E N, Ugolkova E A, Tulyani S, Vincitore A. 2013. Surface tension model for surfactant solutions at the critical micelle concentration. *Journal of Colloid and Interface Science*, **393**, 151–160.

Cárdenas H, Kamrul-Bahrin M A H, Seddon D, Othman J, Cabral J T, Mejía A, Shahruddin S, Matar O K, Müller E A. 2024. Determining interfacial tension and critical micelle concentrations of surfactants from atomistic molecular simulations. *Journal of Colloid and Interface Science*, **674**, 1071–1082.

Chang H, Cui Y, Wei W, Li X, Gao W, Zhao X, Yin S. 2017. Adsorption behavior and wettability by Gemini surfactants with ester bond at polymer-solution-air systems. *Journal of Molecular Liquids*, **230**, 429–436.

Chauhan B S, Namuco O S, Ocampo L A L, Son T N, Thu T A, Nam N N, Phuong L N, Bajwa A A. 2015. Weedy rice (*Oryza sativa* f. spontanea) problems and management in wet direct-seeded rice (*O. sativa* L.) in the Mekong Delta of Vietnam. *Crop Protection*, **78**, 40–47.

Chen G Q, An K, Chen Y, Lu C X, Liu Y Y. 2024. Double-spraying with different routes significantly improved the performance of both pre- and post-emergence wheat herbicides applied by unmanned aerial spraying systems. *Crop Protection*, **176**, 106503.

Chen P, Douzals J P, Lan Y, Cotteux E, Delpuech X, Pouxviel G, Zhan Y. 2022. Characteristics of unmanned aerial spraying systems and related spray drift: A review. *Frontiers in Plant Science*, **13**, 870956.

Cheng X, Wang A, Cao L, Cao C, Zhao P, Yu M, Zheng L, Huang Q. 2024. Efficient delivery of the herbicide quinclorac by nanosuspension for enhancing deposition, uptake and herbicidal activity. *Pest Management Science*, **80**, 4665–4674.

Corrias F, Melis A, Atzei A, Marceddu S, Dedola F, Sirigu A, Pireddu R, Lai F, Angioni A. 2021. Zoxamide accumulation and retention evaluation after nanosuspension technology application in tomato plant. *Pest Management Science*, **77**, 3508–3518.

Deng X, Zhao P, Zhou X, Bai L. 2021. Excellent sustained-release efficacy of herbicide quinclorac with cationic covalent organic frameworks. *Chemical Engineering Journal*, **405**, 126979.

Ding X, Guo L, Du Q, Wang T, Zeng Z, Wang Y, Cui H, Gao F, Cui B. 2024. Preparation and comprehensive evaluation of the efficacy and safety of chlorantraniliprole nanosuspension. *Toxics*, **12**, 78.

Van Eerdenbrugh B, Van den Mooter G, Augustijns P. 2008. Top-down production of drug nanocrystals: Nanosuspension stabilization, miniaturization and transformation into solid products. *International Journal of Pharmaceutics*, **364**, 64–75.

Farooq M, Siddique K H M, Rehman H, Aziz T, Lee D J, Wahid A. 2011. Rice direct seeding: Experiences, challenges and opportunities. *Soil and Tillage Research*, **111**, 87–98.

Gao F, Cui B, Wang C, Li X, Li B, Zhan S, Shen Y, Zhao X, Sun C, Wang C, Wang Y, Zeng Z, Cui H. 2022. Nano-EMB-SP improves the solubility, foliar affinity, photostability and bioactivity of emamectin benzoate. *Pest Management Science*, **78**, 3717–3724.

Gao Y, Guo R, Fan R, Liu Z, Kong W, Zhang P, Du F P. 2018. Wettability of pear leaves from three regions characterized at different stages after flowering using the OWRK method. *Pest Management Science*, **74**, 1804–1809.

Gaudin T, Rotureau P, Pezron I, Fayet G. 2018. Investigating the impact of sugar-based surfactants structure on surface tension at critical micelle concentration with structure-property relationships. *Journal of Colloid and Interface Science*, **516**, 162–171.

Gomez A, Narayan M, Zhao L, Jia X, Bernal R A, Lopez-Moreno M L, Peralta-Videa J R. 2021. Effects of nano-enabled agricultural strategies on food quality: Current knowledge and future research needs. *Journal of Hazardous Materials*, **401**, 123385.

He L, Ding L, Waterhouse G I N, Li B, Liu F, Li P. 2021. Performance matching between the surface structure of cucumber powdery mildew in different growth stages and the properties of surfactant solution. *Pest Management Science*, **77**, 3538–3546.

He X, Bonds J, Herbst A, Langenakens J. 2017. Recent development of unmanned aerial vehicle for plant protection in East Asia. *International Journal of Agricultural and Biological Engineering*, **10**, 18–30.

Huang Z, Wang C, Li Y, Zhang H, Zeng A, He X. 2023. Field evaluation of spray drift and nontargeted soybean injury from unmanned aerial spraying system herbicide application under acceptable operation conditions. *Pest Management Science*, **79**, 1140–1153.

Iqbal N, Thirunavukkarasu S, Krishna R, Hazra D K, Jawale C, Yadav S, Alam S, Ghosh S, Agrawal A, Kumar J. 2023. Environmentally benign design of renewable oleoresin-bioenergized imidacloprid nanohydrocolloids for improved activity, lower toxicity, and agroecological sustainability. *ACS Sustainable Chemistry & Engineering*, **11**, 15480–15491.

Ito A, Konnerth C, Schmidt J, Peukert W. 2016. Effect of polymer species and concentration on the production of mefenamic acid nanoparticles by media milling. *European Journal of Pharmaceutics and Biopharmaceutics*, **98**, 98–107.

Ivanova N A, Starov V M. 2011. Wetting of low free energy surfaces by aqueous surfactant solutions. *Current Opinion in Colloid & Interface Science*, **16**, 285–291.

Jiang T, Duan J, Zhang Z, Xie B, Yang Z. 2023. Performance matching of common pesticides in banana plantations on the surface of banana leaves at different growth stages. *Pest Management Science*, **79**, 5116–5129.

Katzman D, Bohbot-Raviv Y, Dubowski Y. 2021. Does polyacrylamide-based adjuvant actually reduce primary drift of airborne pesticides? *Science of the Total Environment*, **775**, 145816.

Kovalchuk N M, Trybala A, Arjmandi-Tash O, Starov V. 2016. Surfactant-enhanced spreading: Experimental achievements and possible mechanisms. *Advances in Colloid and Interface Science*, **233**, 155–160.

Lee K S, Ivanova N, Starov V M, Hilal N, Dutschk V. 2008. Kinetics of wetting and spreading by aqueous surfactant solutions. *Advances in Colloid and Interface Science*, **144**, 54–65.

Li B, Ren Y, Zhang D X, Xu S, Mu W, Liu F. 2018. Modifying the formulation of abamectin to promote its efficacy on southern root-knot nematode (*Meloidogyne incognita*) under blending-of-soil and root-irrigation conditions. *Journal of Agricultural and Food Chemistry*, **66**, 799–805.

Li B X, Wang W C, Wang K, Zhang D X, Guan L, Liu F. 2015. Thiacloprid suspension formula optimization by a response surface methodology. *RSC Advances*, **5**, 26654–26661.

Li B X, Wang W C, Zhang X P, Zhang D X, Mu W, Liu F. 2017. Integrating uniform design and response surface methodology to optimize thiacloprid suspension. *Scientific Reports*, **7**, 46018.

Li J, Wang Z, Zhang H, Gao J, Zheng A. 2021. Progress in the development of stabilization strategies for nanocrystal preparations. *Drug Delivery*, **28**, 19–36.

Li X X, Liu Y, He L F, Gao Y Y, Mu W, Zhang P, Li B X, Liu F. 2020. Fungicide formulations influence their control efficacy by mediating physicochemical properties of spray dilutions and their interaction with target leaves. *Journal of Agricultural and Food Chemistry*, **68**, 1198–1206.

Li Z, Zhang X, Wang Y, Zheng Z, Zhang C, Wu T, Wu Y, Gao Y, Du F. 2023. Improved method to characterize leaf surfaces, guide adjuvant selection, and improve glyphosate efficacy. *Journal of Agricultural and Food Chemistry*, **71**, 1348–1359.

Liu C, Li C, Bing H, Zhao J, Li L, Sun P, Li T, Du D, Zhao J, Wang X, Xiang W. 2023. Integrated physiological, transcriptomic, and metabolomic analysis reveals the mechanism of guvermectin promoting seed germination in direct-seeded rice under chilling stress. *Journal of Agricultural and Food Chemistry*, **71**, 7348–7358.

Lu Z, Gao Y, Zhang C, Bao Z, Wang W, Lin J, Du F. 2021. Surface properties of *Tetranychus urticae* Koch (Acari: Tetranychidae) and the effect of their infestation on the surface properties of kidney bean (*Phaseolus vulgaris* L.) hosts. *Pest Management Science*, **77**, 5120–5128.

Muthayya S, Sugimoto J D, Montgomery S, Maberly G F. 2014. An overview of global rice production, supply, trade, and consumption. *Annals of the New York Academy of Sciences*, **1324**, 7–14.

Nuruzzaman M, Rahman M M, Liu Y, Naidu R. 2016. Nanoencapsulation, nano-guard for pesticides: A new window for safe application. *Journal of Agricultural and Food Chemistry*, **64**, 1447–1483.

O'Looney N, Fry S C. 2005. The novel herbicide oxaziclomefone inhibits cell expansion in maize cell cultures without affecting turgor pressure or wall acidification. *New Phytologist*, **168**, 323–329.

Oerke E C, Dehne H W. 2004. Safeguarding production-losses in major crops and the role of crop protection. *Crop Protection*, **23**, 275–285.

Ohno H, Banayo N P M C, Bueno C, Kashiwagi J-i, Nakashima T, Iwama K, Corales A M, Garcia R, Kato Y. 2018. On-farm assessment of a new early-maturing drought-tolerant rice cultivar for dry direct seeding in rainfed lowlands. *Field Crops Research*, **219**, 222–228.

Ottis B V, Talbert R E. 2017. Barnyardgrass (*Echinochloa crus-galli*)

control and rice density effects on rice yield components. *Weed Technology*, **21**, 110–118.
Panneerselvam P, Kumar V, Banik N C, Kumar V, Parida N, Wasim I, Das A, Pattnaik S, Roul P K, Sarangi D R, Sagwal P K, Craufurd P, Balwinder S, Yadav A, Malik R K, Singh S, McDonald A J. 2020. Transforming labor requirement, crop yield, and profitability with precision dry-direct seeding of rice and integrated weed management in Eastern India. *Field Crops Research*, **259**, 107961.
Peng S, Huang J, Sheehy J E, Laza R C, Visperas R M, Zhong X, Centeno G S, Khush G S, Cassman K G. 2004. Rice yields decline with higher night temperature from global warming. *Proceedings of the National Academy of Sciences of the United States of America*, **101**, 9971–9975.
Ray D K, Ramankutty N, Mueller N D, West P C, Foley J A. 2012. Recent patterns of crop yield growth and stagnation. *Nature Communications*, **3**, 1293.
Sanyal D, Bhowmik P C, Reddy K N. 2017. Influence of leaf surface micromorphology, wax content, and surfactant on primisulfuron droplet spread on barnyardgrass (*Echinochloa crus-galli*) and green foxtail (*Setaria viridis*). *Weed Science*, **54**, 627–633.
Savary S, Castilla N P, Elazegui F A, Teng P S. 2005. Multiple effects of two drivers of agricultural change, labour shortage and water scarcity, on rice pest profiles in tropical Asia. *Field Crops Research*, **91**, 263–271.
Scholz N, Behnke T, Resch-Genger U. 2018. Determination of the critical micelle concentration of neutral and ionic surfactants with fluorometry, conductometry, and surface tension — A method comparison. *Journal of Fluorescence*, **28**, 465–476.
Shan C, Wu J, Song C, Chen S, Wang J, Wang H, Wang G, Lan Y. 2022. Control efficacy and deposition characteristics of an unmanned aerial spray system low-volume application on corn fall armyworm *Spodoptera frugiperda*. *Frontiers in Plant Science*, **13**, 900939.
Shegokar R, Muller R H. 2010. Nanocrystals: Industrially feasible multifunctional formulation technology for poorly soluble actives. *International Journal of Pharmaceutics*, **399**, 129–139.
Si Y, Yu C, Dong Z, Jiang L. 2018. Wetting and spreading: Fundamental theories to cutting-edge applications. *Current Opinion in Colloid & Interface Science*, **36**, 10–19.
Song Y C, Wang S J, Du Y H, Li Z Y, Yuan Y M, Chen Y H, Wang W W, Dong H Q, Huo Z Y, Liang Y. 2026. Development of biodegradable triple-stimuli-responsive mesoporous organosilica nanocarriers for targeted pesticide delivery and enhanced plant immunity in rice disease management. *Journal of Integrative Agriculture*, **25**, 2496–2509.
Sun Z, Zhao R, Yu M, Liu Y, Ma Y, Guo X, Gu Y C, Formstone C, Xu Y, Wu X. 2023. Enhanced dosage delivery of pesticide under unmanned aerial vehicle condition for peanut plant protection: Tank-mix adjuvants and formulation improvement. *Pest Management Science*, **80**, 1632–1644.
Suzuki H, Jikihara K, Sonoda M, Usui Y. 2003. Development of a new herbicide, oxaziclomefone. *Journal of Pesticide Sciences*, **28**, 221–222.
Tang Q, Sun Y, Li J, Zhou M, Yang D, Pang Y. 2024. Preparations of 25 wt% of pyraclostrobin nanosuspension concentrate (SC) using lignosulfonate-based colloidal spheres to improve its thermal storage stability. *Molecules*, **29**, 1419.
Tian Y, Wang S, Yu Y, Sun W, Fan R, Shi J, Gu W, Wang Z, Zhang H, Zheng A. 2022. Review of nanosuspension formulation and process analysis in wet media milling using microhydrodynamic model and emerging characterization methods. *International Journal of Pharmaceutics*, **623**, 121862.
Wang D, Saleh N B, Byro A, Zepp R, Sahle-Demessie E, Luxton T P, Ho K T, Burgess R M, Flury M, White J C, Su C. 2022. Nano-enabled pesticides for sustainable agriculture and global food security. *Nature Nanotechnology*, **17**, 347–360.
Wang L, Xia S, Zhang H, Li Y, Huang Z, Qiao B, Zhong L, Cao M, He X, Wang C, Liu Y. 2024. Tank-mix adjuvants improved spray performance and biological efficacy in rice insecticide application with unmanned aerial vehicle sprayer. *Pest Management Science*, **80**, 4371–4385.
Wang P, Lombi E, Zhao F J, Kopittke P M. 2016. Nanotechnology: A new opportunity in plant sciences. *Trends in Plant Science*, **21**, 699–712.
Wang S, He X, Song J, Wang S, Jia X, Ling Y. 2018. Effects of xanthan gum on atomization and deposition characteristics in water and Silwet 408 aqueous solution. *International Journal of Agricultural and Biological Engineering*, **11**, 29–34.
Wang Y, Zheng Y, Zhang L, Wang Q, Zhang D. 2013. Stability of nanosuspensions in drug delivery. *Journal of Controlled Release*, **172**, 1126–1141.
Xiao D, Cheng J, Liang W, Cheng C, Wang Q, Chai R, Yan Z, Du Y, Zhao J. 2019. Innovative approach to nano thiazole-Zn with promising physicochemical and bioactive properties by nanoreactor construction. *Journal of Agricultural and Food Chemistry*, **67**, 11577–11583.
Yang C W, Xie G, Yuan L, Hu Y, Sheng G P. 2024. Harnessing multiscale physiochemical interactions on nanobiointerface for enhanced stress resilience in rice. *ACS Nano*, **18**, 14617–14628.
Yu B, Cheng J, Fang Y, Xie Z, Xiong Q, Zhang H, Shang W, Wurm F R, Liang W, Wei F, Zhao J. 2024. Multi-stimuli-responsive, topology-regulated, and lignin-based nano/microcapsules from pickering emulsion templates for bidirectional delivery of pesticides. *ACS Nano*, **18**, 10031–10044.
Zhang C, Li S S, Yang F, Hu R F. 2026. Does the adoption of direct-seeded rice affect pesticide use? Evidence from China. *Journal of Integrative Agriculture*, **25**, 366–376.
Zhang C, Zhao X, Lei J, Ma Y, Du F. 2017. The wetting behavior of aqueous surfactant solutions on wheat (*Triticum aestivum*) leaf surfaces. *Soft Matter*, **13**, 503–513.
Zhang Q. 2007. Strategies for developing Green Super Rice. *Proceedings of the National Academy of Sciences of the United States of America*, **104**, 16402–16409.
Zhang R, Hewitt A J, Chen L, Li L, Tang Q. 2023. Challenges and opportunities of unmanned aerial vehicles as a new tool for crop pest control. *Pest Management Science*, **79**, 4123–4131.
Zhang S, Bao Z, Wu Y, Wang Y, Liu R, Gao Y, Zhao X, Zhang C, Du F. 2023. Enhancing the stability and effectivity of multiple pesticide formulation mixtures by adding an eco-friendly adjuvant. *ACS Sustainable Chemistry & Engineering*, **11**, 15385–15396.
Zhang X, Xiong L. 2021. Effect of adjuvants on the spray droplet size of pesticide dilute emulsion. *Colloids and Surfaces A*: *Physicochemical and Engineering Aspects*, **619**, 126557.
Zhao C, Liu B, Piao S, Wang X, Lobell D B, Huang Y, Huang M, Yao Y, Bassu S, Ciais P, Durand J L, Elliott J, Ewert F, Janssens I A, Li T, Lin E, Liu Q, Martre P, Müller C, Peng S, *et al*. 2017. Temperature increase reduces global yields of major crops in four independent estimates. *Proceedings of the National Academy of Sciences of the United States of America*, **114**, 9326–9331.
Zhao K, Hu J, Ma Y, Wu T, Gao Y, Du F. 2019. Topology-regulated pesticide retention on plant leaves through concave Janus carriers. *ACS Sustainable Chemistry & Engineering*, **7**, 13148–13156.
Zhao R, Yu M, Sun Z, Li L J, Shang H Y, Xi W J, Li B, Li Y Y, Xu Y, Wu X M. 2022. Using tank-mix adjuvant improves the physicochemical properties and dosage delivery to reduce the use of pesticides in unmanned aerial vehicles for plant protection in wheat. *Pest Management Science*, **78**, 2512–2522.
Zheng L, Cao C, Li R Y, Cao L D, Zhou Z L, Li M, Huang Q L. 2018. Preparation and characterization of water-in-oil emulsions of isoprothiolane. *Colloids and Surfaces A*: *Physicochemical and Engineering Aspects*, **537**, 399–410.
Zhou B, Xie K P, Iqbal M A, Ali T. 2026. Drivers and barriers to unmanned aerial vehicle (UAV) adoption in agriculture: Evidence from Jiangxi Province, China. *Journal of Integrative Agriculture*, **25**, 2201–2213.
Zhu F, Cao C, Cao L, Li F, Du F, Huang Q. 2019. Wetting behavior and maximum retention of aqueous surfactant solutions on tea leaves. *Molecules*, **24**, 2094.
Zhu Y Q, Yu C X, Li Y, Zhu Q Q, Zhou L, Cao C, Yu T T, Du F P. 2014. Research on the changes in wettability of rice (*Oryza sativa*) leaf surfaces at different development stages using the OWRK method. *Pest Management Science*, **70**, 462–469.

Executive Editor-in-Chief Fanghao Wan
Managing Editor Juan Zhang